Fortschr. Phys. 65, No. 6–8, 1600025 (2017) / DOI 10.1002/prop.201600025

Fortschritte der Physik
Progress of Physics

Original Paper

On the role of the electric dipole moment in the diffraction of biomolecules at nanomechanical gratings

*Christian Knobloch[1], Benjamin A. Stickler[2], Christian Brand[1], Michele Sclafani[1], Yigal Lilach[3], Thomas Juffmann[1,**], Ori Cheshnovsky[3], Klaus Hornberger[2], and Markus Arndt[1,*]*

Received 8 March 2016, accepted 27 June 2016
Published online 7 September 2016

We investigate effects of a permanent electric dipole moment on matter-wave diffraction at nanomechanical gratings. Specifically, the diffraction patterns of hypericin at ultra-thin carbonaceous diffraction masks are compared with those of a polar and a non-polar porphyrin derivative of similar mass and de Broglie wavelength. We present a theoretical analysis of the diffraction of a rotating dipole highlighting that small local electric charges in the material mask can strongly reduce the interference visibility. We discuss the relevance of this finding for single grating diffraction and multi-grating interferometry with biomolecules.

1 Introduction

Nanomechanical gratings [1] have played a major role in matter-wave interferometry since the first diffraction experiments with atoms. They were used to study a variety of atomic [2–5] and molecular systems [6], as well as weakly bound van der Waals clusters [2, 7]. Ring-shaped periodic structures in thin membranes also proved useful as Fresnel zone plates [8, 9]. Such experiments with a single diffraction element were soon complemented by closed interferometers [10–12] used to investigate the influence of decoherence [13–15], inertial forces [16], and the interaction with external fields [17, 18].

Material gratings are often regarded as universal since the periodic beam depletion is seemingly independent of the internal structure of the particle. This generality is, however, impaired by attractive interactions between the grating and the diffracted molecule, such as the Casimir-Polder interaction. The influence of van der Waals forces can be reduced by using gratings with a thickness of a few nanometers, or even masks made of single-layer graphene [19].

Yet, electric charges on the grating may still lead to phase averaging of the de Broglie wave. Earlier studies showed that electron waves above a metal may experience decoherence [20–23]. A broadening of the diffraction orders was observed for slow electrons diffracted at material gratings [24, 25]. For polar molecules, a dipole-charge interaction has also been seen to reduce the quantum fringe contrast in earlier interferometric deflection experiments [26].

In the present article we investigate effects of a permanent electric dipole moment on matter-wave diffraction at material gratings. This is of particular importance for quantum interference experiments with biomolecules, most of which come with a permanent electric dipole moment due to the functional groups required for molecular recognition. We find that the presence of residual charges on the grating mask can give rise to surprisingly effective contrast reduction caused by phase averaging due to the rotating dipole.

We start by demonstrating quantum diffraction of hypericin at a grating made of amorphous carbon. Hypericin is a naturally occurring antiviral, antidepressant and anti-inflammatory substance [27], discussed as a photosensitizer in photodynamic tumor therapy [28, 29]. We compare the molecular diffraction pattern of hypericin to that of a polar and a non-polar tetraphenylporphyrin derivative in order to assess the influence of its dipole moment. We then provide a model for the diffraction of polar particles at thin, charged gratings, accounting for the thermal rotation of the molecular dipole in the electrostatic field of these surface charges. Finally, we discuss

[1] University of Vienna, Faculty of Physics, VCQ, QuNaBioS, Boltzmanngasse 5, A-1090, Vienna, Austria
[2] Faculty of Physics, University of Duisburg-Essen, Lotharstraße 1, 47048, Duisburg, Germany
[3] The Center for Nanosciences and Nanotechnology and School of Chemistry, The Raymond and Beverly Faculty of Exact Sciences, Tel Aviv University, Tel Aviv, 69978, Israel
* Corresponding author E-mail: Markus.Arndt@univie.ac.at
** Present address: Stanford University, Physics Department, 382 Via Pueblo Mall, Stanford, CA 94305-4060, USA

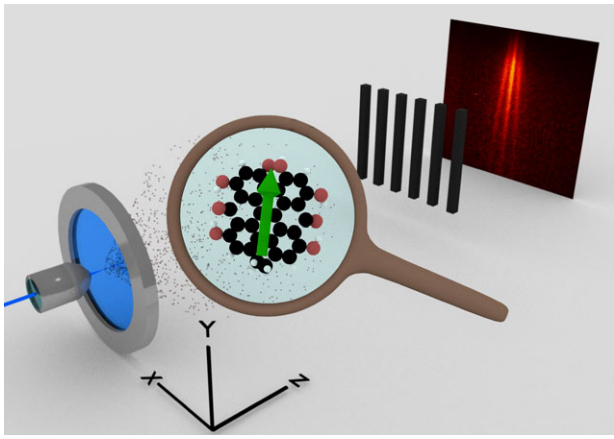

Figure 1 Molecules evaporated by a focused laser from a coated source window propagate in z-direction towards the grating where they are diffracted. They impinge on a quartz plate further downstream and are visualized by laser-induced fluorescence. The magnifier shows an artist's view on hypericin and its permanent electric dipole moment.

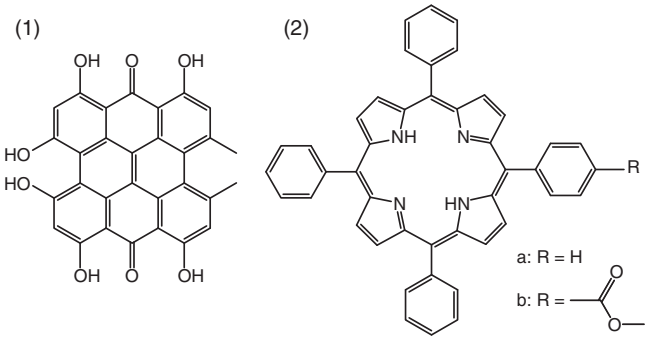

Figure 2 Chemical structure of the molecules used for matter-wave diffraction experiments: Hypericin (1), TPP (2a) and MeOTPP (2b).

alternative reasons for the observed signal reduction and conclude that electric charges are a probable source.

2 Experimental setup

The experimental apparatus is sketched in Fig. 1 and described in detail in [30]. We use meso-tetraphenylporphyrin (TPP, Porphyrin Systems, purity > 98%), 5-(4-methoxycarbonylphenyl)-10,15,20-triphenylporphyrin (MeOTPP, TCI-Scientific, purity > 90%) and hypericin (AvaChem Scientific, purity > 98%) as purchased, without further purification (see Fig. 2). The molecular samples are dissolved in acetone to prepare a homogeneous film on a vacuum entrance window after solvent evaporation.

A continuous desorption laser beam (421 nm, 62 mW) is focused to a spot with a waist of 1.6±0.1 μm at the inner surface of the coated window. The small size of the source ensures that the evaporated molecules exhibit a transverse coherence of around 5 μm at the position of the grating, 1555 mm downstream. The molecular beam is collimated to 10 μrad by two slits before it passes the nanomechanical grating.

Two different gratings were used: A first grating with a periodicity of 100 nm was milled into a 21 nm thick amorphous carbon membrane (TEMwindows) [30]. A second grating was milled into an 8 nm thick SiO_2 matrix with a periodicity of 160 nm (TedPella).

After the diffraction process the molecules propagate through vacuum before they are absorbed on a quartz plate 585 mm behind the grating. They are observed in laser-induced fluorescence. In different runs, each molecular species is optically excited by a laser that matches its absorption spectrum. TPP and MeOTPP are excited at 661 nm, while radiation at 532 nm is used for hypericin. The resulting fluorescence is collected by a 20-fold microscope objective and imaged onto a UV-enhanced CCD camera (LOT ORIEL iXon 885-KCS-VP).

3 Experimental results

In Fig. 3 a we show the molecular pattern obtained for hypericin diffracted at the carbon grating. Three dominant diffraction peaks can be observed which have an intensity maximum at a molecular velocity around 250 m/s. The height dependence in the separation of the diffraction orders is due to the fact that slower molecules fall deeper in the gravitational field of the earth before they hit the detector. Comparing this diffraction pattern to the one of TPP (Fig. 3 b), one observes that the signal of hypericin is diffusely broadened: the individual diffraction orders are wider than for TPP. This is illustrated by the intensity distributions at different velocities accompanying the diffraction images in Fig. 3.

For TTP the width of the individual diffraction orders increases slightly with velocity while for hypericin the opposite trend is observed. Since TPP and hypericin are chemically rather different, we repeat the experiment with MeOTPP. The molecules TPP and MeOTPP are structurally very similar. The main difference, apart from a small mass difference (TPP: $m = 614.8$ amu, MeOTPP: $m = 672.8$ amu) is that MeOTPP has a permanent electric dipole moment of about 1.8 D due to the benzoic acid methyl ester side group [31], as evaluated numerically. As shown in Fig. 3 c, we observe the broadening of the diffraction peaks also for MeOTPP. For the fast

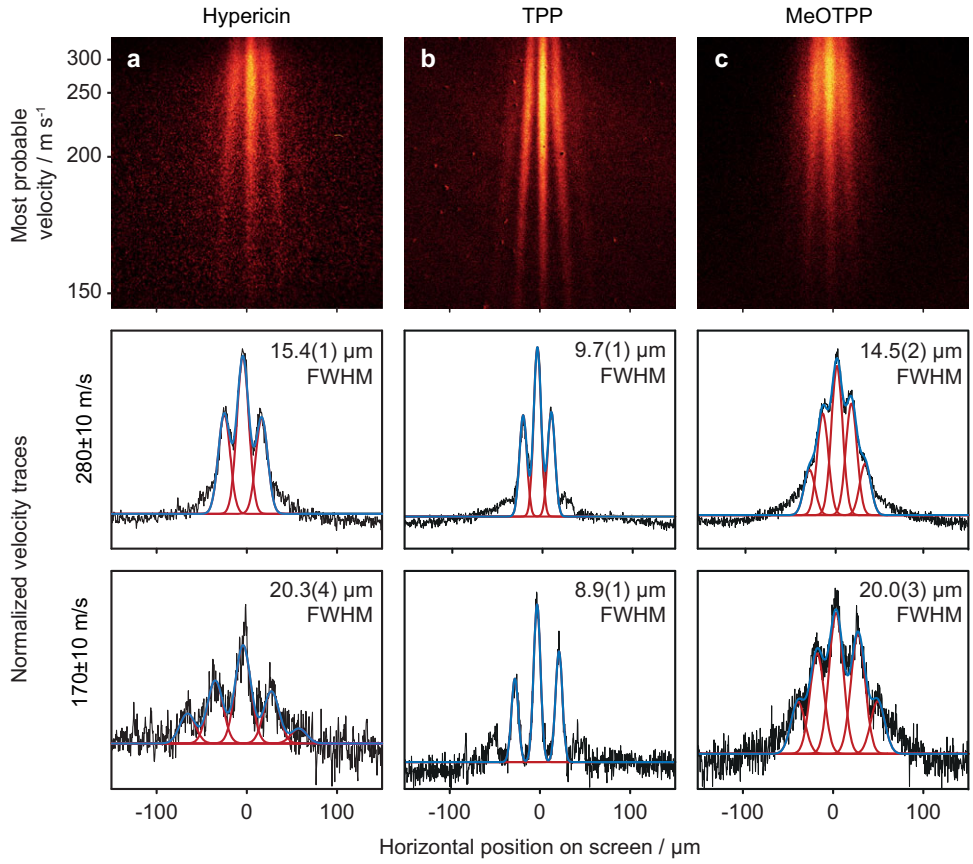

Figure 3 Molecular diffraction images of (a) hypericin, (b) TPP and (c) MeOTPP. In the lower panels the respective intensity distributions for fast (middle, 270-290 m/s) and slow velocity classes (bottom, 160-180 m/s) are shown. For each trace the FWHM of the diffraction peaks is given as extracted from a Gaussian fit to a common line width.

velocity class the full width at half maximum (FWHM) of the diffraction peaks is 9.7 ± 0.1 μm for TPP and 14.5 ± 0.2 μm for MeOTPP. As stated before, the diffraction orders of slow TPP molecules get narrower which can be explained by their higher transversal coherence. For MeOTPP, however, their width increases from 14.5 ± 2 μm to 20.0 ± 0.3 μm.

In order to test whether the visibility reduction is related to the interaction with the grating, we repeated the diffraction experiments for TPP and MeOTPP with a grating made of silicon dioxide (SiO_2) instead of amorphous carbon. This is motivated by their difference in the electric conductivity. The respective diffraction patterns and intensity distributions are shown in Fig. 4. The diffraction orders are spaced more closely, because the period of this grating is 160 nm compared to 100 nm for the carbon grating. Nevertheless, one can clearly distinguish the diffraction orders for TPP. For MeOTPP individual diffraction orders can no longer be identified and the observed signal resembles the envelope of the single slit diffraction pattern.

Note that the SiO_2 grating is much thinner than the carbon gratings (8 nm compared to 20 nm) and has a larger geometrical slit width (82 nm) compared to the carbon mask (55 nm). This suggests that van der Waals forces are not responsible for the observed contrast reduction. On the other hand, we observe a stronger population of higher order diffraction peaks in the case of SiO_2, which indicates a more pronounced particle-wall interaction in the case of the dielectric mask.

While our observations suggest that the visibility reduction is due to dipole-grating interactions, other dipole-related mechanisms are also conceivable that give rise to a beam broadening. One possible reason for a contrast reduction is a potential increase in the effective source size. However, both the measured laser focus and depleted molecular traces on the desorption window rule out this effect. Moreover, molecules with a permanent dipole moment might also diffuse more rapidly on the detector plate than non-polar particles. This was tested by depositing molecules through a narrow slit in front of the detector plate. The width of the transmitted

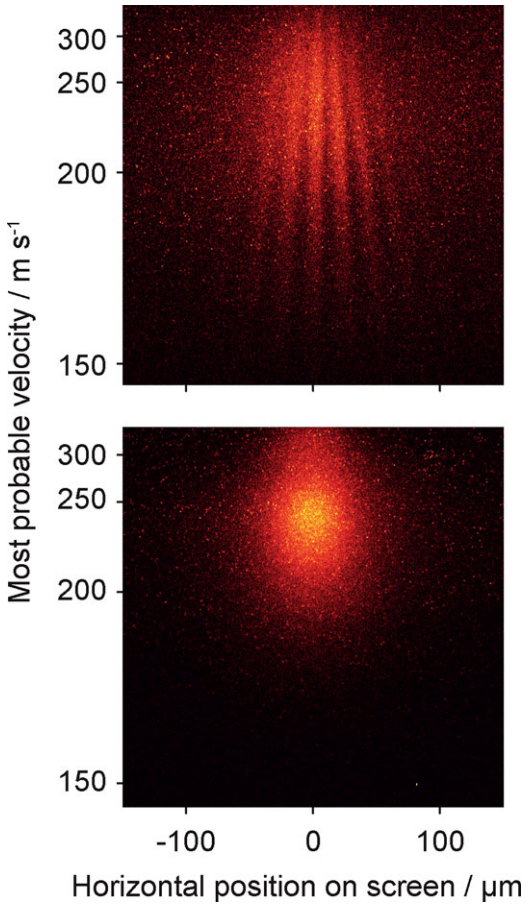

Figure 4 Molecular diffraction images of TPP (top) and MeOTPP (bottom) at the silicon dioxide grating.

stripe was independent of the molecular species which excluded an increase in surface diffusion. Finally, collisions with gas molecules can also lead to the suppression of quantum interference [15], and the influence of the molecular dipole moment on collisional decoherence was discussed in [32]. However, tests in the current setup showed that the momentum transfer from a single gas particle is sufficient to deflect the molecule way beyond the small detection region (400×400 μm^2), leaving the contrast unaffected.

In summary, our experimental findings imply that the dipole and velocity-dependent contrast reduction must be caused by interactions with the grating. Given that the gratings were milled with a focused gallium ion beam, which is known to deposit surface charges [33], it is likely that charges were implanted into the membrane during the patterning process. This is also consistent with discrepancies that were found between the observed and predicted Casimir-Polder interactions at nanomechanical silicon nitride gratings [34]. In the following section, we present a theory that evaluates the possible role of residual charges in the diffraction of polar molecules.

4 Theory

In order to determine the influence of grating charges on the interference pattern, we consider a polar symmetric-top molecule characterized by the three moments of inertia $I_1 = I_2 = I \neq I_3$ as well as an electric dipole moment d_0. We denote its center-of-mass (CM) position by $\mathbf{r}$ and its orientational degrees of freedom (DOFs) by Ω. The molecule is thermally emitted with longitudinal velocity v_z from a point-like source (located at $z = 0$), diffracted from an infinitesimally thin, charged grating of transverse extension ℓ_x (at $z = L$) and finally detected at the screen (at $z = 2L$). Denoting the grating direction as x, we can neglect the y-dependence since the extension of the grating in this direction exceeds the spatial coherence of the particle. Since the longitudinal kinetic energy exceeds the transverse kinetic energy and the average grating potential by orders of magnitude in a typical experiment, it can be described in the eikonal approximation [35]. Thus, the longitudinal CM coordinate $z = v_z t$ is effectively eliminated and the transverse state operator ρ_{2L} at the detector is related to the transverse state operator ρ_0 at the source by successive application of the free time evolution from the source to the grating, the grating transformation $\hat{t}$ and the free time evolution to the detection screen, respectively. Tracing out the orientational DOFs then yields the interference pattern.

The grating transformation operator $\hat{t}$ maps the state ρ_L in front of the grating onto the state ρ'_L directly after the grating, $\rho_L \mapsto \rho'_L = \hat{t}\rho_L\hat{t}^\dagger$. The influence of the grating mask can be modeled with the help of the aperture function $|t(x)| \in \{0, 1\}$, which is unity within the grating slits and zero elsewhere [36]. On the other hand, the phase imprinted onto the molecular state while it is traversing the grating depends on the interaction potential between the grating and the molecule. For simplicity we assume that the dominant interaction is due to homogeneously distributed surface charges on the grating. They create an electric field which reaches out along the z-direction. Thus, the interaction potential is

$$V(x, z, \Omega) = -d_0\mathbf{m}(\Omega) \cdot \mathbf{E}(x, z), \tag{1}$$

where $\mathbf{m}(\Omega)$ is the orientation of the molecular dipole moment and $\mathbf{E}(x, z)$ is the electric field due to the charges.

In a more realistic description of the interaction between molecule and grating, one would add the

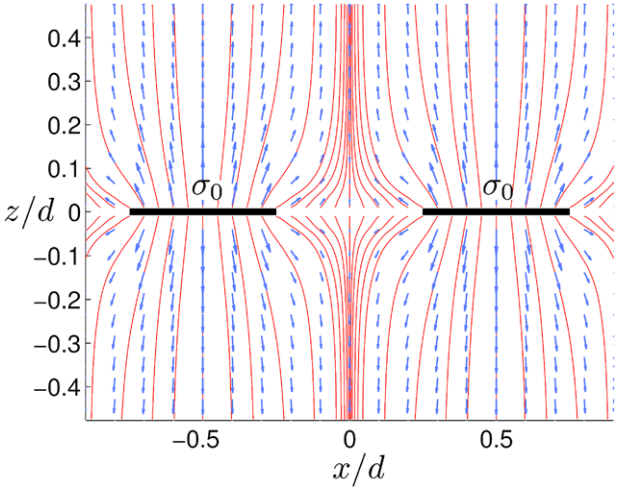

Figure 5 Electric field lines of a thin, homogeneously charged grating of period d, surface charge density σ_0 and opening fraction $f = 1/2$.

dispersive Casimir-Polder interaction [34] to the potential (1), which is not included in the present model. The electrostatic field $\mathbf{E}(x, z)$ can be calculated from Coulomb's law applied to a thin grating with surface charge density σ_0, period d, opening fraction f and width ℓ_x [37]. The resulting field is depicted in Fig. 5. For moderate charge densities the potential energy of the molecular dipole in the field is much lower than the mean rotational energy $k_B T$. Since the orientational DOFs are initially thermally distributed at a high temperature, the molecule rotates freely while traversing the field and we can utilize the free rotor approximation [38]. This means that the phase shift for each rotation state $|\ell mk\rangle$ of the molecule is obtained by integrating the expectation value of the potential energy in this rotation state along the straight eikonal trajectory [38]. For the case of a thin grating the explicit calculation shows that the phase shift takes the particularly simple form

$$\phi(x) = \Delta\phi \left[\frac{x}{d} - \frac{f}{2} \mathrm{tri}\left(\frac{x}{d}\right) \right], \tag{2}$$

where $\Delta\phi = (1-f) d_0 \sigma_0 d/\hbar\varepsilon_0 v_z$ is the maximal phase difference between two neighboring slits. Here, we denote by $\mathrm{tri}(x)$ a 1-periodic triangular wave with

$$\mathrm{tri}(x) := \begin{cases} 2x/f & \text{for } 2|x|/f \le 1, \\ \left[\mathrm{sgn}(x) - 2x\right]/(1-f) & \text{for } 2|x|/f > 1, \end{cases} \tag{3}$$

for $x \in [-1/2, 1/2)$ and we take the center of the coordinate system to be the center of the grating. The resulting grating transformation operator can thus be written as

$$\hat{t} = |t(\hat{x})| \sum_{\ell=0}^{\infty} \sum_{m,k=-\ell}^{\ell} e^{i\phi(\hat{x}) Q_{\ell mk}} \otimes |\ell mk\rangle\langle \ell mk|, \tag{4}$$

where $Q_{\ell mk} = mk/\ell(\ell+1)$ is the expectation value of $\cos\hat{\theta}$ in the state $|\ell mk\rangle$ [39–41], with θ the angle between the dipole and the grating axis. Here we assumed for simplicity that the molecular dipole is aligned with the molecule's symmetry axis. Extending the current model to the cases where the dipole is not aligned with the symmetry axis of the molecule is straightforward, although the resulting expressions will be more complicated [38].

The grating transformation (4) is the thermal average of angular momentum dependent grating transformations with angular momentum dependent phase shifts. The phase (2) consists of a linear and a periodic contribution, which compensate each other within each grating slit, so that the maximal phase difference between two neighboring slits is $\Delta\phi$. The periodic contribution $\mathrm{tri}(x)$ to the eikonal phase (2) describes an alternating phase modulation of the matter-wave for each fixed expectation value $Q_{\ell mk}$, while the linear contribution describes a transverse momentum kick, experienced by the molecule due to its interaction with the charged grating. This momentum kick can shift the interference pattern either to the left or the right. In particular, for fixed $Q_{\ell mk}$ the transferred momentum is $(1-f) d_0 \sigma_0 Q_{\ell mk}/v_z \varepsilon_0$ and its direction is determined by the quantum numbers m and k. The average over the quantum numers ℓ, m and k then leads to phase averaging and thus the signal contrast is reduced. Relation (2) implies that the effect is relevant as soon as $\Delta\phi \simeq 2\pi$.

In order to evaluate the interference pattern, one successively evaluates the free propagation from the source to the grating, the grating transformation and the flight from the grating to the screen. In the end, the orientational DOFs are traced out. Using that they are thermally distributed at a very high temperature, $T \gg \hbar^2/\tilde{I} k_B$ with $\tilde{I}$ the dominant moment of inertia of the particle, we can replace the sum over the discrete values $Q_{\ell mk}$ by an integral over the continuous classical mean value $q = \langle \cos\theta \rangle \in [-1, 1]$ [38].

The thermal distribution $p_{\mathrm{th}}(q)$ of q gives the statistical weight of each phase shift $q\Delta\phi$. It is shown in the Appendix that

$$p_{\mathrm{th}}(q) = \frac{1}{2} - \frac{1}{2}\sqrt{\frac{I}{I_3}} \left[\frac{1}{\sqrt{1-(1-I/I_3)\, q^2}} + \ln\left(\frac{(1+\sqrt{I/I_3})|q|}{1+\sqrt{1-(1-I/I_3)\, q^2}} \right) \right], \tag{5}$$

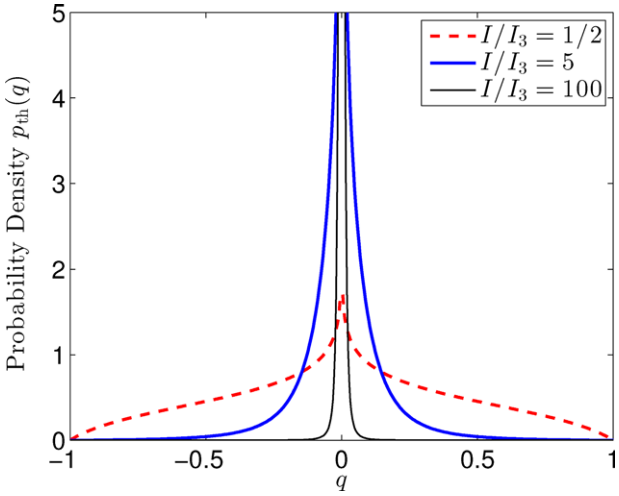

Figure 6 The probability distribution of the classical dynamic mean value $q = \langle \cos\theta \rangle$ (5) for $I/I_3 = 1/2$ (very oblate symmetric top), $I/I_2 = 5$ (slightly prolate symmetric top) and $I/I_3 = 100$ (very prolate symmetric top).

as depicted in Fig. 6. This distribution is independent of the temperature T and it is a function of the ratio I/I_3 between the molecule's two independent moments of inertia. For $I/I_3 \to 1/2$ (thin disc) the distribution is broad, while it approaches the δ-distribution for $I/I_3 \to \infty$ (linear rotor).

The resulting interference pattern at the detection screen can then be written as

$$S(x) \propto \int_{-1}^{1} \mathrm{d}q\, p_{\rm th}(q) \left| \int_{-\infty}^{\infty} \mathrm{d}x'\, |t(x')| e^{i\phi(x')q} \times \exp\left[-i \frac{2\pi x'(x-x')}{d\Delta x} \right] \right|^2 . \quad (6)$$

Here, $\Delta x = 2\pi\hbar L/Mv_z d$ is the distance between two neighboring diffraction peaks in the far field, *i.e.* for $\ell_x^2/\Delta x d \ll 1$. In the far field, the position space integration in Eq. (6) can be carried out explicitly and the signal for an N-slit grating is

$$S(x) \propto \mathrm{sinc}^2\left(\frac{\pi f x}{\Delta x}\right) \times \int_{-1}^{1} \mathrm{d}q\, p_{\rm th}(q)\, \frac{\sin^2\left[\pi N\left(x/\Delta x - q\Delta\phi/2\pi\right)\right]}{\sin^2\left[\pi\left(x/\Delta x - q\Delta\phi/2\pi\right)\right]} . \quad (7)$$

This expression shows that the charge-free N-slit interference pattern gets blurred by the distribution $p_{\rm th}$. From this relation it is apparent that phase averaging can become important for $\Delta\phi \gtrsim 2\pi$.

In Fig. 7 we show the theoretically expected interference pattern for a prolate symmetric top molecule for three different charge densities. One observes that the signal contrast is significantly reduced even for moderate charge densities.

5 Discussion

Our experiment demonstrates that polar molecules are more prone to dephasing at nanomechanical diffraction gratings than non-polar but similarly polarizable objects. The effect is more pronounced for slow particles. This is consistent with our model of charged gratings which predicts a velocity-dependent broadening of the diffraction orders. We therefore attribute the leading dephasing mechanism for polar molecules at our nanomechanical gratings to local residual charges. Our observation may also be relevant for earlier experiments with polar particles which did not discuss this effect explicitly [30, 42].

The charges are most likely deposited during the fabrication process. Charge densities up to 10^{13} e/cm^2 were found in silicon nitride irradiated with a gallium ion beam [33]. While the electric conductivity of amorphous carbon depends on a number of parameters like fabrication, thickness and temperature, its value exceeds the respective value for SiO_2 by several orders of magnitude. Hence, electric charges implanted in SiO_2 are less likely to be neutralized and should result in stronger electric fields than in amorphous carbon. Eliminating the influence of local charges is ambitious since even

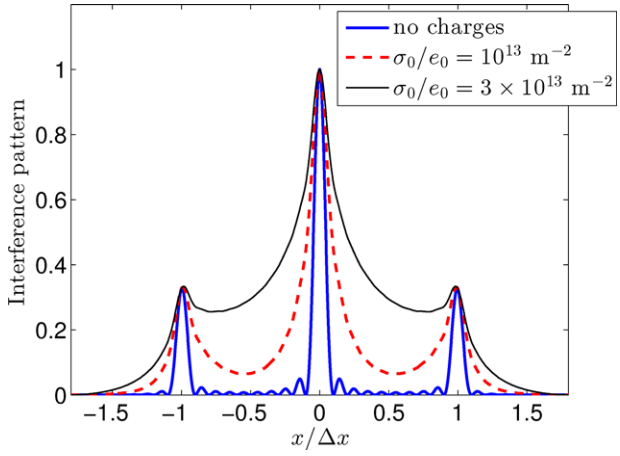

Figure 7 Theoretically expected far-field interference pattern of a prolate symmetric-top molecule ($M = 505$ amu, $I/I_3 = 10$) with dipole moment $\mu_0 = 4$ D [43], motivated by the experiment with hypericin, for three different charge densities σ_0. The molecular velocity is $v_z = 280$ m/s, the distance $L = 585$ mm, the opening fraction $f = 0.55$ and the grating period $d = 100$ nm.

nanometer-sized metal layers do not suffice to shield the fields and nearby grating support structures may also carry charges.

6 Conclusion

Our experimental results indicate that the interaction between residual charges in a nanomechanical diffraction mask and polar molecules can cause a significant loss of visibility in quantum interference. The comparison between two different grating materials shows that this effect is more dramatic for gratings with higher surface charge density (SiO_2). The theoretically predicted phase-averaging due to the rotation of the molecular dipole is qualitatively consistent with the experimental results.

We find that the use of material gratings as coherent manipulation elements in quantum optics becomes increasingly challenging for particles of high polarity. This suggests that future interferometry with large polar biomolecules will require at least one optical grating. However, when working with incoherent molecular sources, at least one absorptive grating is usually required to prepare the required spatial coherence. Nanomechanical masks can still serve this purpose even though they imprint field-induced phase shifts. In Talbot-Lau near-field interferometry [12] phase shifts and attractive forces in the first of three gratings do not scramble the final interference contrast, they may even enhance it by narrowing the effective slit transmission function. Molecules with a very large dipole moment may be removed from the beam only if the local grating attraction becomes too strong.

Acknowledgments. We acknowledge support by the European Commission (304886), the European Research Council (320694) and the Austrian science funds (DK CoQuS W1210-3). CB acknowledges the financial support of the Alexander von Humboldt foundation through a Feodor Lynen fellowship. TJ acknowledges support by the Gordon and Betty Moore Foundation. We thank Stefan Scheel and Johannes Fielder (Univ. Rostock) for fruitful discussions and Lisa Wörner for assistance in measurements.

Appendix

A Statistics of free rotations

In this appendix we derive the classical thermal distribution $p_{\rm th}(q)$ of the dynamic mean value $q = \langle\cos\theta\rangle$ for symmetric top molecules as required for our purposes. This distribution determines the probability density of deflection angles of polar particles traversing an inhomogeneous field of moderate strength [44–46]. In order to calculate $p_{\rm th}(q)$, we consider a free symmetric top, with the classical Hamilton function

$$H_{\rm rot}(\Omega, p_\Omega) = \frac{1}{2I}\left(\frac{(p_\varphi - p_\psi\cos\theta)^2}{\sin^2\theta} + p_\theta^2\right) + \frac{p_\psi^2}{2I_3}, \qquad \text{(A.1)}$$

where $\Omega = (\varphi, \theta, \psi)$ are the Euler angles in the z-y'-z'' convention, $p_\Omega = (p_\varphi, p_\theta, p_\psi)$ are the canonically conjugate momenta and $1/2 < I/I_3 < \infty$. The three conserved quantities of the free rotor dynamics are the rotational energy (A.1) and the two angular momenta p_φ and p_ψ, and they define the classical rotation state of the body. The dynamic mean value $\langle\cos\theta\rangle$ can be calculated by separation of variables and subsequent integration:

$$\langle\cos\theta\rangle = \frac{1}{\tau_{\rm rot}}\int_0^{\tau_{\rm rot}} {\rm d}t\,\cos\theta(t) = \frac{p_\varphi p_\psi}{2E_{\rm rot}I + p_\psi^2\,(1 - I/I_3)}, \qquad \text{(A.2)}$$

where the rotational period $\tau_{\rm rot}$ of θ-rotations is given by [38]

$$\tau_{\rm rot} = \frac{2\pi I}{\sqrt{2E_{\rm rot}I + p_\psi^2(1 - I/I_3)}}. \qquad \text{(A.3)}$$

We note the close resemblance between the classical mean value (A.2) and the quantum mechanical expectation value $Q_{\ell mk} = mk/\ell(\ell+1)$.

The thermal distribution $p_{\rm th}(q)$ of the mean value $q = \langle\cos\theta\rangle$ is defined by

$$p_{\rm th}(q) = \int {\rm d}\Omega\,{\rm d}p_\Omega\,\delta[q - \langle\cos\theta\rangle]\,p_{\rm th}(\Omega, p_\Omega), \qquad \text{(A.4)}$$

where $p_{\rm th}(\Omega, p_\Omega)$ is the Boltzmann distribution of the rotational energy (A.1). The distribution (A.4) can be evaluated by following the derivation presented in [38], and a straightforward calculation yields the probability density (5). It is normalized, even and independent of the temperature T. Thus its first moment $\langle q\rangle$ vanishes and its second moment can be calculated to be

$$\langle q^2\rangle = \frac{1}{3}\frac{1}{1 - I/I_3}\left(1 - \sqrt{\frac{I}{I_3}}\frac{\arcsin\sqrt{1 - I/I_3}}{\sqrt{1 - I/I_3}}\right). \qquad \text{(A.5)}$$

The second moment is strictly decreasing for increasing I/I_3 and in the limit $I/I_3 \to \infty$ (linear rotor) it tends towards zero. For instance, for spherical tops, $I/I_3 = 1$, we have $\langle q^2\rangle = 1/9$. In the linear rotor limit $I/I_3 \to \infty$ the distribution (5) approaches the δ-distribution, $p_{\rm th}(q) \to$

$\delta(q)$, and the mean value $\langle \cos\theta \rangle$ vanishes for all rotation states.

Key words. Matter-wave interferometry, biomolecules, dephasing, hypericin, dipole moment.

References

[1] D. W. Keith, M. L. Schattenburg, H. I. Smith, and D. E. Pritchard, *Phys. Rev. Lett.* **61**, 1580 (1988).
[2] W. Schöllkopf and J. P. Toennies, *Science* **266**, 1345 (1994).
[3] J. D. Perreault, A. D. Cronin, and T. A. Savas, *Phys. Rev. A* **71**, 053612 (2005).
[4] R. E. Grisenti, W. Schöllkopf, J. P. Toennies, G. C. Hegerfeldt, and T. Köhler, *Phys. Rev. Lett.* **83**, 1755 (1999).
[5] V. P. A. Lonij, C. E. Klauss, W. F. Holmgren, and A. D. Cronin, *Phys. Rev. Lett.* **105**, 233202 (2010).
[6] M. Arndt, O. Nairz, J. Vos-Andreae, C. Keller, G. van der Zouw, and A. Zeilinger, *Nature* **401**, 680 (1999).
[7] R. E. Grisenti, W. Schöllkopf, J. P. Toennies, G. C. Hegerfeldt, T. Köhler, and M. Stoll, *Phys. Rev. Lett.* **85**, 2284 (2000).
[8] R. B. Doak, R. E. Grisenti, S. Rehbein, G. Schmahl, J. P. Toennies, and C. Wöll, *Phys. Rev. Lett.* **83**, 4229 (1999).
[9] T. Reisinger, S. Eder, M. M. Greve, H. I. Smith, and B. Holst, *Microelectron. Eng.* **87**, 1011 (2010).
[10] D. W. Keith, C. R. Ekstrom, Q. A. Turchette, and D. E. Pritchard, *Phys. Rev. Lett.* **66**, 2693 (1991).
[11] J. F. Clauser and S. Li, *Phys. Rev. A* **49**, R2213 (1994).
[12] B. Brezger, L. Hackermüller, S. Uttenthaler, J. Petschinka, M. Arndt, and A. Zeilinger, *Phys. Rev. Lett.* **88**, 100404 (2002).
[13] M. S. Chapman, T. D. Hammond, A. Lenef, J. Schmiedmayer, R. A. Rubenstein, E. Smith, and D. E. Pritchard, *Phys. Rev. Lett.* **75**, 3783 (1995).
[14] L. Hackermüller, K. Hornberger, B. Brezger, A. Zeilinger, and M. Arndt, *Nature* **427**, 711 (2004).
[15] K. Hornberger, S. Uttenthaler, B. Brezger, L. Hackermüller, M. Arndt, and A. Zeilinger, *Phys. Rev. Lett.* **90**, 160401 (2003).
[16] A. Lenef, T. D. Hammond, E. T. Smith, M. S. Chapman, R. A. Rubenstein, and D. E. Pritchard, *Phys. Rev. Lett.* **78**, 760 (1997).
[17] C. Ekstrom, J. Schmiedmayer, M. Chapman, T. Hammond, and D. Pritchard, *Phys. Rev. A* **51**, 3883 (1995).
[18] M. Berninger, A. Stefanov, S. Deachapunya, and M. Arndt, *Phys. Rev. A* **76**, 013607 (2007).
[19] C. Brand, M. Sclafani, C. Knobloch, Y. Lilach, T. Juffmann, J. Kotakoski, C. Mangler, A. Winter, A. Turchanin, J. Meyer, O. Cheshnovsky, and M. Arndt, *Nat. Nanotechnol.* **10**, 845 (2015).
[20] P. Sonnentag and F. Hasselbach, *Phys. Rev. Lett.* **98**, 200402 (2007).
[21] J. R. Anglin, J. P. Paz, and W. H. Zurek, *Phys. Rev. A* **55**, 4041 (1997).
[22] Y. Levinson, *J. Phys. A: Math. Gen.* **37**, 3003 (2004).
[23] P. Machnikowski, *Phys. Rev. B* **73**, 155109 (2006).
[24] G. Gronniger, B. Barwick, H. Batelaan, T. Savas, D. Pritchard, and A. Cronin, *Appl. Phys. Lett.* **87**, 124104 (2005).
[25] B. J. McMorran and A. D. Cronin, *New J. Phys.* **11**, 033021 (2009).
[26] S. Eibenberger, S. Gerlich, M. Arndt, J. Tüxen, and M. Mayor, *New J. Phys.* **13**, 43033 (2011).
[27] Z. Saddiqe, I. Naeem, and A. Maimoona, *J. Ethnopharmacol.* **131**, 511 (2010).
[28] P. Agostinis, A. Vantieghem, W. Merlevede, and P. A. M. de Witte, *Int. J. Biochem. Cell Biol.* **34**, 221 (2002).
[29] T. A. Theodossiou, J. S. Hothersall, P. A. de Witte, A. Pantos, and P. Agostinis, *Mol. Pharm.* **6**, 1775 (2009).
[30] T. Juffmann, A. Milic, M. Müllneritsch, P. Asenbaum, A. Tsukernik, J. Tüxen, M. Mayor, O. Cheshnovsky, and M. Arndt, *Nat. Nanotechnol.* **7**, 297 (2012).
[31] E. Saiz, J. P. Hummel, P. J. Flory, and M. Plavsic, *J. Phys. Chem.* **85**, 3211 (1981).
[32] K. Walter, B. A. Stickler, and K. Hornberger, *Phys. Rev. A* **93**, 063612 (2016).
[33] S. Yogev, J. Levin, M. Molotskii, A. Schwarzman, O. Avayu, and Y. Rosenwaks, *J. Appl. Phys.* **103**, 064107 (2008).
[34] C. Brand, J. Fiedler, T. Juffmann, M. Sclafani, C. Knobloch, S. Scheel, Y. Lilach, O. Cheshnovsky, and M. Arndt, *Ann. Phys. (Berlin)* **527**, 580 (2015).
[35] S. Nimmrichter and K. Hornberger, *Phys. Rev. A* **78**, 023612 (2008).
[36] M. Born and E. Wolf, Principles of Optics (Pergamon Press, Oxford, 1993).
[37] J. D. Jackson, Classical Electrodynamics (Wiley, New York, 1999).
[38] B. A. Stickler and K. Hornberger, *Phys. Rev. A* **92**, 023619 (2015).
[39] C. H. Townes and L. Schawlow, Microwave Spectroscopy (Dover, New York, 1975).
[40] A. R. Edmonds, Angular Momentum in Quantum Mechanics (Princeton University Press, Princeton, 1996).
[41] D. M. Brink and G. Satchler, Angular Momentum (Oxford Science Publications, Oxford, 2002).
[42] W. Schöllkopf, R. E. Grisenti, and J. P. Toennies, *EPJ D* **28**, 125 (2004).
[43] C. Etzlstorfer and H. Falk, *Chem. Month.* **129**, 855 (1998).
[44] E. Gershnabel and I. Sh. Averbukh, *Phys. Rev. Lett.* **104**, 153001 (2010).
[45] E. Gershnabel and I. Sh. Averbukh, *J. Chem. Phys.* **135**, 084307 (2011).
[46] E. Gershnabel and I. Sh. Averbukh, *J. Chem. Phys.* **134**, 054304 (2011).